

Riemannian quantum circuit optimization based on matrix product operators

Isabel Nha Minh Le^{1,*}, Shuo Sun¹ and Christian B. Mendl^{1,2,†}

¹*Technical University of Munich, School of Computation,*

Information and Technology, Boltzmannstraße 3, 85748 Garching, Germany

²*Technical University of Munich, Institute for Advanced Study, Lichtenbergstraße 2a, 85748 Garching, Germany*

(Dated: January 16, 2025)

We significantly enhance the simulation accuracy of initial Trotter circuits for Hamiltonian simulation of quantum systems by integrating first-order Riemannian optimization with tensor network methods. Unlike previous approaches, our method imposes no symmetry assumptions, such as translational invariance, on the quantum systems. This technique is scalable to large systems through the use of a matrix product operator representation of the reference time evolution propagator. Our optimization routine is applied to various spin chains and fermionic systems, with a particular focus on one-dimensional systems described by the transverse-field Ising Hamiltonian, the Heisenberg Hamiltonian, and the spinful Fermi-Hubbard Hamiltonian. In these cases, our approach achieves a relative error improvement of up to four orders of magnitude. Furthermore, we demonstrate the versatility of our method by applying it to molecular systems, specifically lithium hydride, achieving an error improvement of up to eight orders of magnitude. This proof of concept highlights the potential of our approach for broader applications in quantum simulations.

I. INTRODUCTION

Simulating the time evolution of a quantum system was the original motivation behind quantum computers [1] and remains one of their most natural applications [2, 3], particularly in quantum chemistry and quantum many-body physics [4–6]. A widely used method for this purpose is Trotterization [7, 8], where the time propagator $U_t = e^{-iHt}$ is approximated using lower-body operators. This approach is straightforward to implement and comes in various orders, each with different circuit depths and error scalings [8]. However, achieving high accuracy for long-time simulations necessitates deep quantum circuits. This raises some interesting questions:

- Can the same quantum circuit layout provided by Trotterization achieve better accuracy?
- And is it possible to optimize the quantum gates using only classical computation so that expensive quantum resources are only needed for the (optimized) Hamiltonian simulation?

These questions have been previously explored by (i) considering specific parameterizations of the quantum gates [9–12], and (ii) directly interpreting the quantum gates as unitary matrices in a brickwall circuit [13–15]. In this work, we focus on the latter approach.

In Ref. [13], Riemannian optimization and tensor network methods are combined to globally optimize the quantum gates under the constraint of unitarity for small translationally-invariant quantum systems using an explicit full-rank matrix reference of U_t . Due to the translational invariance, the same optimized quantum gates can

simulate the quantum dynamics of corresponding larger systems. In contrast, Refs. [14, 15] employ a local quantum gate optimization inspired by tensor network methods to directly optimize larger quantum systems. To this end, they approximate U_t using a fine Trotterization for a suitable time step t , allowing it to be expressed efficiently as a matrix product operator (MPO). The classically optimized quantum circuit can then repeatedly be executed on quantum hardware to enable the simulation of quantum dynamics for longer times $t' \gg t$.

This work integrates the ideas and methods of Refs. [13–15]. Specifically, we focus on quantum systems where a Trotter step can be represented as a brickwall circuit and introduce a global optimization method to enhance quantum gates under the constraint of unitarity. To achieve this, we adapt the gradient-based ADAM optimizer [16] to the framework of Riemannian optimization on the complex Stiefel manifold, i.e., the manifold of unitary matrices. We approximate the time evolution reference operator U_t to target larger quantum systems by employing a higher-order Trotterization MPO and evaluate the cost function and corresponding gradient utilizing tensor network methods. Our Riemannian optimization approach updates the quantum gates of the quantum circuit globally in contrast to the local gate updates used in Refs. [14, 15], and does not assume any symmetry invariance as in Ref. [13]. We apply the presented method to exemplary spin chains and fermionic systems. Specifically, we conduct numerical experiments on systems of 50 qubits for a non-integrable case of the Ising Hamiltonian and a Heisenberg model, explicitly considering non-translationally invariant systems. For fermionic systems, we utilize the fermionic swap network [17] and optimize a one-dimensional spinful Fermi-Hubbard model of 50 spin orbitals, as well as a paradigmatic example of lithium hydride (LiH) for the molecular Hamiltonian.

Recently, we became aware of the independently developed work of Rogerson and Roy [18]. Their study

* isabel.le@tum.de

† christian.mendl@tum.de

combines the Riemannian ADAM optimizer, automatic differentiation, and tensor network methods to optimize a quantum state represented as a matrix product state. In contrast, our research takes a different approach: we directly optimize the time evolution operator, allowing for an arbitrary choice of initial quantum state and analytically implementing the required gradient without relying on additional software packages for automatic differentiation.

II. OPTIMIZATION PROBLEM

Quantum circuit layout. We consider a so-called brickwall circuit layout built from L layers of two-qubit gates, where the ℓ -th layer of the quantum circuit W^ℓ has n_ℓ gates. We denote the i -th gate in layer W^ℓ as G_i^ℓ and the concatenation of layers i to j as $W^{i:j}$, i.e.,

$$W^\ell = \bigotimes_{i=1}^{n_\ell} V_i^\ell \quad \text{and} \quad W^{i:j} = \prod_{\ell=i}^j W^\ell.$$

Finally, we call the overall brickwall circuit $W = W^{1:L}$.

Cost function. When considering a quantum circuit W of N qubits, the Frobenius norm can be used to quantify how well W approximates a reference unitary U_{ref} via

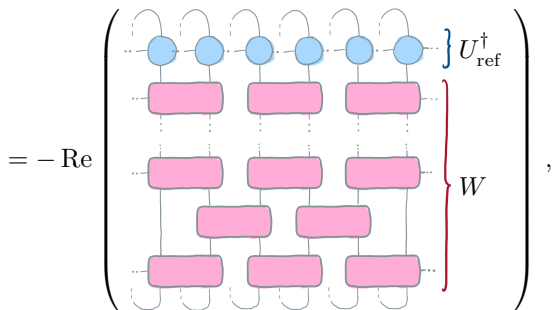
$$\mathcal{C}(U_{\text{ref}}, W) = \frac{1}{2 \cdot 2^N} \|U_{\text{ref}} - W\|_F^2, \quad (1)$$

where the Frobenius norm can be expressed as

$$\begin{aligned} \|U_{\text{ref}} - W\|_F^2 &= \text{Tr} [(U_{\text{ref}} - W)^\dagger (U_{\text{ref}} - W)] \\ &= 2 \cdot 2^N - 2 \text{Re} \text{Tr} [U_{\text{ref}}^\dagger W]. \end{aligned}$$

From the latter, the variational part of \mathcal{C} can be extracted, which we denote as

$$\mathcal{L}(U_{\text{ref}}, W) = -\text{Re} \text{Tr} [U_{\text{ref}}^\dagger W], \quad (2)$$



where the last line is a diagrammatic interpretation in the context of tensor networks.

Formulation of optimization problem. The objective is to optimize a set of unitary two-qubit gates $G = \{G_i\}_{i \in \text{ind}(W)}$ such that the resulting optimized brickwall circuit W minimizes its distance to the reference U_{ref} .

The underlying optimization problem can hence be expressed as

$$G_{\text{opt}} = \arg \min_{G \in \mathcal{U}(4)^{\times N}} \mathcal{C}(U_{\text{ref}}, W). \quad (3)$$

In the latter, $\mathcal{U}(4)$ denotes the set of unitary 4×4 -matrices:

$$\mathcal{U}(4) = \{G_g \in \mathbb{C}^{4 \times 4} | G_g^\dagger G_g = \mathbb{1}_4\}, \quad (4)$$

which can be viewed as a particular case of the complex Stiefel manifold.

Quantum circuit initialization. Previous analyses have shown that a good initialization can significantly enhance quantum circuit optimization [13–15]. Depending on the chosen model and simulation time, higher-order Trotterizations do not always yield a better approximation error than lower-order Trotterizations. When optimizing a brickwall circuit with L layers, we first determine which order of Trotterization matches the number of layers to achieve the best approximation error. We additionally allow the extension of Trotter circuits by adding identity layers. For example, if we aim to optimize a brickwall circuit with L layers, which could be initialized as a second-order Trotter circuit, $U_{\text{Trotter}}^{\text{II}}(L)$, but a shallower fourth-order circuit, $U_{\text{Trotter}}^{\text{IV}}(L')$, with $L' < L$ layers exist with a more minor approximation error

$$\mathcal{C}(U_{\text{ref}}, U_{\text{Trotter}}^{\text{IV}}(L')) < \mathcal{C}(U_{\text{ref}}, U_{\text{Trotter}}^{\text{II}}(L)),$$

then we initialize the quantum circuit as the fourth-order Trotter circuit with L' layers and extend this quantum circuit by $L - L'$ layers consisting of identity two-qubit gates.

III. RIEMANNIAN OPTIMIZATION ON THE COMPLEX STIEFEL MANIFOLD

As described above, the goal is to optimize a set of two-qubit gates under the constraint of unitarity, which means working on the complex Stiefel manifold. One effective method for such optimization is the gradient-based Riemannian optimization, which does not necessitate any specific parameterization of the unitary gates. Recently, this approach has been explicitly utilized for various optimization tasks in quantum technologies [13, 18–25]. In the following, we will provide a brief overview of the basic concepts required for Riemannian optimization of brickwall circuits. For a more detailed introduction to these concepts, we refer interested readers to Refs. [26–28]. Furthermore, we adapt the well-known ADAM optimizer [16] to the setting of Riemannian optimization.

A. Concepts of Riemannian geometry

Intuitively, a manifold \mathcal{M} can be thought of as a curved space that, at any point, $x \in \mathcal{M}$, can be locally described

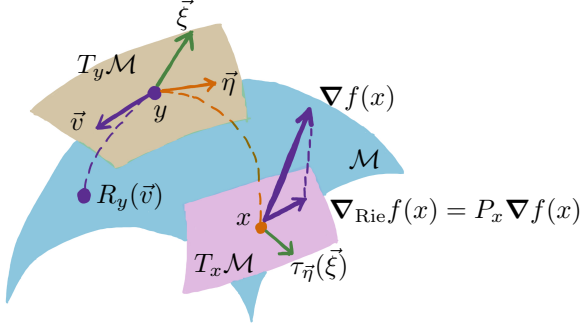


Figure 1: Visualization of concepts on the Riemannian manifold \mathcal{M} . A point $y \in \mathcal{M}$ is “moved” in the direction of the vector $\vec{v} \in T_y \mathcal{M}$ via the retraction R . A vector $\vec{\xi}$ is moved in the direction of a vector $\vec{\eta} \in T_x \mathcal{M}$ to the tangent space $T_x \mathcal{M}$ in point $x \in \mathcal{M}$ using the vector transport τ . Lastly, the Riemannian gradient $\nabla_{\text{Rie}} f(x)$ can be obtained as the projected Euclidean gradient $\nabla f(x)$ through the projector P .

by a Euclidean space, which is isomorphic to a vector space called the *tangent space* $T_x \mathcal{M}$. The collection of all points in the manifold and the corresponding tangent spaces, $(x, T_x \mathcal{M})$, is called the *tangent bundle* $T\mathcal{M}$. If each tangent space is equipped with an inner product $\langle \cdot, \cdot \rangle_x : T_x \mathcal{M} \rightarrow T_x \mathcal{M}$, \mathcal{M} and $\langle \cdot, \cdot \rangle$ form a *Riemannian manifold*. When naively moving a point $x \in \mathcal{M}$ along the direction of a vector $\vec{v}_x \in T_x \mathcal{M}$, the resulting point will, in general, lie in $T_x \mathcal{M}$ and not be an element of \mathcal{M} anymore. A *retraction*

$$R : T\mathcal{M} \rightarrow \mathcal{M}, R_x(\vec{v}_x) = y$$

is a smooth map from the tangent bundle into the manifold, and hence $R_x(v_x)$ corresponds to moving a point x in the direction of v_x within the manifold. Moreover, a so-called *vector transport*

$$\tau_{\vec{\eta}_x} : T_x \mathcal{M} \rightarrow T_y \mathcal{M}, \tau_{\vec{\eta}_x}(\vec{v}_x) = \vec{v}_y$$

is a smooth map that moves a vector $\vec{v}_x \in T_x \mathcal{M}$ to another tangent space $T_y \mathcal{M}$ in point $y \in \mathcal{M}$, where $\vec{\eta}_x \in T_x \mathcal{M}$ is the direction of transport. Consider a Riemannian manifold \mathcal{M} and a function $f : \mathcal{M}^{\times n} \rightarrow \mathbb{R}$ with inputs $x = \{x_i\}_{i=1}^n$ from a product manifold. The so-called *Riemannian gradient* can be obtained from the Euclidean gradient $\nabla f(x)$ by projecting the latter entry-wise onto $T_x \mathcal{M}^{\times n}$ via some suitable projection P :

$$\nabla_{\text{Rie}} f(x) = P_x \nabla f(x) \in T_x \mathcal{M}^{\times n}.$$

An overview of these concepts is visualized in Fig. 1.

B. Example of the complex Stiefel manifold

As already mentioned, \mathcal{U} defined in Eq. (4) is a manifold, and the tangent space in a point $G \in \mathcal{U}$ can be

parameterized by a set of complex anti-Hermitian matrices

$$T_G \mathcal{U} = \{GA : A \in \mathbb{C}^{m \times m}, A^\dagger = -A\}.$$

Furthermore, a Riemannian metric can be defined on each tangent space $T_G \mathcal{U}$ by

$$\langle \cdot, \cdot \rangle : T_G \mathcal{U} \times T_G \mathcal{U} \rightarrow \mathbb{R}, \quad \langle X, Y \rangle_G = \text{Tr}(X^\dagger Y),$$

with which \mathcal{U} can be identified as a Riemannian manifold and – more specifically – a particular case of the complex Stiefel manifold. A proper *retraction of \mathcal{U}* is induced by the polar decomposition $A = UM$ with U being a unitary matrix and M being a positive semi-definite Hermitian matrix. When denoting the corresponding unitary part as $\pi(A) = U$, a vector $\vec{\xi} \in T_G \mathcal{U}$ can be retracted into the unitary manifold via

$$R^{\text{polar}} : T\mathcal{U} \rightarrow \mathcal{U}, \quad R_G^{\text{polar}}(\vec{\xi}) = \pi(G + \vec{\xi}). \quad (5)$$

A general vector $\vec{\eta} \in \mathbb{C}^{m \times m}$ can be *projected onto the tangent space* $T_G \mathcal{U}$ by means of the linear projector

$$\begin{aligned} P_G(\vec{\eta}) &= \vec{\eta} - \frac{1}{2}V(\vec{\eta}^\dagger X + G^\dagger \vec{\eta}) \\ &= G \text{skew}(G^\dagger \vec{\eta}). \end{aligned} \quad (6)$$

Utilizing Eq. (6), the map

$$\tau_{\vec{\eta}}(\vec{\xi}) = P_{R_G^{\text{polar}}(\vec{\eta})}(\vec{\xi}) \quad (7)$$

is a valid *vector transport on \mathcal{U}* . In other words, a vector $\vec{\xi} \in T_G \mathcal{M}$ in the tangent space corresponding to $G \in \mathcal{M}$ is transported in the direction of $\vec{\eta} \in T_G \mathcal{M}$ by projecting it onto the tangent space corresponding to the retracted directional vector $R_G^{\text{polar}}(\vec{\eta}) \in \mathcal{U}$ using Eq. (6).

When optimizing a brickwall circuit W consisting of $|W|$ two-qubit gates $\{G_i\}_{i \in \text{ind}(W)}$, the cost function f is defined on the product manifold $\mathcal{U}^{\times |W|}$

$$f : \mathcal{U}^{\times |W|} \rightarrow \mathbb{R}.$$

The corresponding tangent space is given by the direct sum of the individual tangent spaces

$$T_W \mathcal{U}^{\times |W|} = \bigoplus_{i \in \text{ind}(W)} T_{G_i}(\mathcal{U}).$$

Using the same projector as given in Eq. (6) the corresponding *Riemannian gradient* can be computed via

$$\nabla_{\text{Rie}} f(W) = P_W \nabla f(W). \quad (8)$$

Lastly, the overall retraction corresponds to applying the retraction in Eq. (5) to the individual quantum gates and tangent vectors.

C. Adapting the ADAM optimizer to the Riemannian setting of the complex Stiefel manifold

In the following, we make use of the previously introduced concepts to adapt the first-order gradient-based ADAM optimizer [16] to the Riemannian optimization setting on the manifold of unitary operations [29]. ADAM aims to minimize an objective function f via the component-wise update rule

$$x_{t+1} \leftarrow x_t - \alpha m_t / \sqrt{v_t},$$

where $\alpha \in \mathbb{R}$ is the learning rate, and m_t and v_t are the first and second momenta in each iteration t , which can be obtained from the gradient ∇f as

$$m_t = \beta_1 m_{t-1} + (1 - \beta_1) \nabla f,$$

$$v_t = \beta_2 v_{t-1} + (1 - \beta_2) (\nabla f)^2,$$

where usually $\beta_1 = 0.9$ and $\beta_2 = 0.99$ are chosen. To constrain ADAM to the unitary manifold, firstly, ∇f has to be replaced by $\nabla_{\text{Rie}} f$, from which follows that v_t is computed from the inner product $\langle \nabla_{\text{Rie}} f, \nabla_{\text{Rie}} f \rangle_{x_t}$. Additionally, some further modifications need to be made.

Vector transport of momentum. m_t is computed by adding the scaled Riemannian gradient $\nabla_{\text{Rie}} f \in T_{x_t} \mathcal{M}$ to the scaled previous momentum $m_{t-1} \in T_{x_{t-1}} \mathcal{U}$, i.e., two quantities from different tangent spaces. Therefore, it is necessary to transport m_{t-1} to the tangent space of the current point. The modified Riemannian momenta updates are then given by

$$\tilde{m}_t = \beta_1 \tau_{\tilde{m}_t}(\tilde{m}_{t-1}) + (1 - \beta_1) \nabla_{\text{Rie}} f,$$

$$\tilde{v}_t = \beta_2 \tau_{\tilde{v}_t}(\tilde{v}_{t-1}) + (1 - \beta_2) \langle \nabla_{\text{Rie}} f, \nabla_{\text{Rie}} f \rangle_{x_t}.$$

Retraction of updated step. Since the Riemannian momenta determine the update direction, the updated point x_{t+1} will lie in the tangent space of the former point x_t . Therefore, the retraction given in Eq. (5) must be applied to obtain valid new parameters within \mathcal{M} . The modified update rule is hence given by

$$\tilde{x}_{t+1} \leftarrow R_{\tilde{x}_t}^{\text{polar}} \left(\tilde{x}_t - \alpha \tilde{m}_t / \sqrt{\tilde{v}_t} \right) \in \mathcal{M}.$$

Note that the ADAM optimizer and its Riemannian adaption are invariant under gradient rescaling.

IV. TENSOR NETWORKS METHODS FOR QUANTUM CIRCUIT OPTIMIZATION

In order to solve the optimization problem formulated in Eq. (3), a reference operator representing the time evolution propagator $U_t = e^{-iHt}$ is required. While U_t can be computed for small systems via numerically exact diagonalization, this approach is infeasible for larger systems of interest due to the curse of dimensionality. Therefore, we choose to approximate U_t to a reasonable accuracy and efficiently express it as an MPO with a maximum bond dimension χ_{max} [14, 15].

A. Matrix product operator representation of the reference time evolution operator

Computing the reference matrix product operator. For the optimization, it is essential to have an efficient and accurate representation of the time evolution operator $U_t = e^{-iHt}$ as a reference, which we will denote as U_{ref} . Depending on the number of qubits N , the references are generated in two different ways:

- For system sizes of $N \leq 12$, we can compute U_t numerically exactly as a full-rank matrix and decompose and truncate it to an MPO.
- For larger systems, we obtain an accurate approximation of U_t using n repetitions of a fourth-order Trotterization $U_{\text{Trotter}}^{\text{IV},n}$. For this purpose, n is chosen such that $U_{\text{Trotter}}^{\text{IV},n}$ has a negligible approximation error for the systems considered in this work. We then treat the resulting deep quantum circuit as a tensor network and contract it into an MPO [14, 15]. To this end, we start with an initial identity MPO and sequentially merge the layers of $U_{\text{Trotter}}^{\text{IV},n}$ into it.

In both cases, the bond dimensions of the MPO are truncated to some maximum value χ_{max} [30], and we denote the resulting MPO by $U_{\chi_{\text{max}}}$ to indicate this property. In practice, the accuracy of U_{ref} does not have to be arbitrarily high. Suppose the final error between the optimized quantum circuit and the reference is $\mathcal{C}_{\text{final}}$. In that case, it is sufficient to have a reference operator U_{ref} that approximates the exact time evolution U_t by

$$\mathcal{C}(U_t, U_{\text{ref}}) \approx \frac{\mathcal{C}_{\text{final}}}{10} = \epsilon_{\text{thres}}.$$

To further relax computational demands, a reasonable target error $\mathcal{C}_{\text{final}}$ is evaluated, and $U_{\chi_{\text{max}}}$ is compressed to the smallest bond dimension $\chi \leq \chi_{\text{max}}$ [15] for which it still holds that

$$\mathcal{C}(U_{\chi_{\text{max}}}, U_{\chi}) \leq \epsilon_{\text{thres}}.$$

The compression is achieved by applying a singular value decomposition (SVD) sweep on $U_{\chi_{\text{max}}}$ in mixed-canonical form, where the canonical center is always moved to the local tensor that is currently truncated [30].

Quantifying the reference approximation error. Several error sources lead to a deviation of U_{ref} from U_t .

- Trotterization error ϵ_{Trot} when approximating U_t by $U_{\text{Trotter}}^{\text{IV},n}$ for systems with $N > 12$ qubits.
- Truncation error ϵ_{trunc} when computing $U_{\chi_{\text{max}}}$.
- Compression error ϵ_{comp} when compressing $U_{\chi_{\text{max}}}$ to U_{χ} , which is given by the chosen ϵ_{thres} .

To estimate the approximation error ϵ_{Trot} , we note that for local Hamiltonians, the error is expected to scale linearly in system size. Hence, ϵ_{Trot} for large system sizes

can be estimated from extrapolating the approximation errors of a Trotterization for a considered simulation time t for small enough systems, for which the exact full-rank matrix U_t can still be computed. In order to quantify the truncation error $\varepsilon_{\text{trunc}}$ of $U_{\chi_{\text{max}}}$, a series of MPOs $\{U_\chi\}_{\chi > \chi_{\text{max}}}$ is computed as described before. First, it is verified that increasing the bond dimension does not change the MPO significantly:

$$\mathcal{C}(U_\chi, U_{\chi+1}) < 10^{-10}.$$

The $\varepsilon_{\text{trunc}}$ of $U_{\chi_{\text{max}}}$ is then given by $\mathcal{C}(U_{\chi_{\text{max}}}, U_{\chi_{\text{max}}+1})$. Lastly, the compression error $\varepsilon_{\text{comp}}$ is determined by the choice of ϵ_{thres} . This study compares the optimization results with Trotterizations up to the fourth order. Hence, $\varepsilon_{\text{comp}}$ is chosen such that the reference MPO is accurate enough to reproduce the error scaling behavior of these Trotter circuits. We will accordingly document the error estimations of the U_{ref} used in the numerical simulations.

B. Tensor network methods for cost function and gradient evaluation

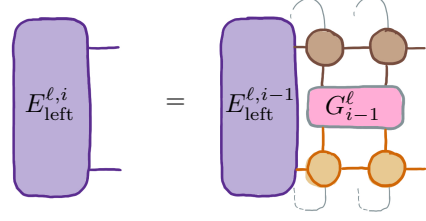
Computing the gradient in the context of tensor networks. Naturally, computing derivatives of the cost function is essential for gradient-based optimization. The gradient of Eq. (1) and Eq. (2) are equal up to a constant factor, and hence the quantity of interest is given by $\nabla \mathcal{L}$, from which $\nabla_{\text{Rie}} \mathcal{L}$ can be obtained by the projection shown in Eq. (6). Following Ref. [13], $\nabla \mathcal{L}$ can be evaluated as

$$\nabla \mathcal{L} = -\text{Tr} \left[U_{\text{ref}}^\dagger \partial_{G_i^\ell} W \right]_{\substack{\ell=1, \dots, L \\ i=1, \dots, n_\ell}}^* \quad (9)$$

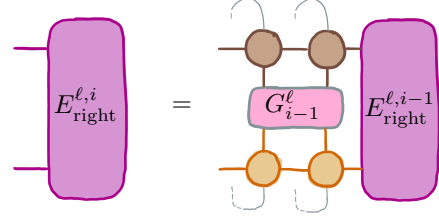
where we denote the number of layers in the brickwall circuit with L and the number of gates in layer ℓ with n_ℓ . When interpreting the brickwall circuit as a tensor network, the partial derivatives $\partial \text{Tr} [U_{\text{ref}}^\dagger W] / \partial G_i^\ell$ can be obtained by “cutting out” the respective quantum gate G_i^ℓ from Eq. (2). This is visualized in Fig. 2.

Identifying tensor networks environments. In order to compute $\nabla \mathcal{L}$, we follow an approach similar to Ref. [15]. For the partial derivative $\partial \mathcal{L} / \partial G_i^\ell$ with respect to the i -th quantum gate in layer ℓ , we first compute a top environment MPO E_{top}^ℓ , which is obtained by merging all layers $\ell' = \ell + 1, \dots, L$ lying above the considered layer ℓ into the adjoint reference MPO U_{ref}^\dagger . Similarly, a bottom environment MPO E_{bottom}^ℓ is computed by merging all layers $\ell' = 1, \dots, \ell - 1$ below the considered layer ℓ . This leads to our layer ℓ being “sandwiched” by the two MPOs E_{top}^ℓ and E_{bottom}^ℓ as visualized in Fig. 2. To contract this resulting tensor network, two further environments are computed. The first results from contracting all tensors to the left of the considered gate G_i^ℓ , which we call the left environment $E_{\text{left}}^{\ell, i}$. Similarly, the right environment $E_{\text{right}}^{\ell, i}$ is obtained by contracting all tensors to the right of G_i^ℓ .

Environment caching. For the efficient evaluation of $\nabla \mathcal{L}$, it is helpful to cache the previous environments. Note that for a fixed layer ℓ , all left environments $E_{\text{left}}^{\ell, i}$ (right environments $E_{\text{right}}^{\ell, i}$) can be recursively obtained by a left-to-right (right-to-left) sweep, since

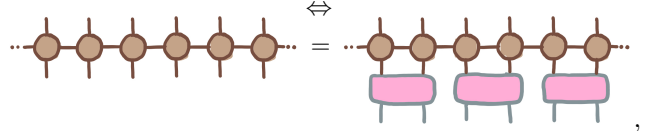


and



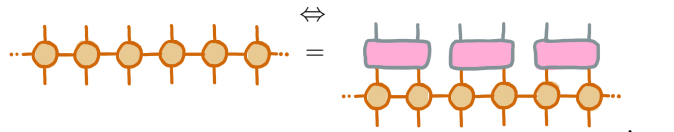
Furthermore, E_{top}^ℓ (E_{bottom}^ℓ) for all layers $\ell = 1, \dots, L$ in the brickwall circuit can be recursively computed by a top-to-bottom (bottom-to-top) sweep, since

$$E_{\text{top}}^{\ell-1} = E_{\text{top}}^\ell W^\ell$$



and

$$E_{\text{bottom}}^{\ell+1} = E_{\text{bottom}}^\ell W^\ell$$



with the initial environments $E_{\text{top}}^L = U_{\text{ref}}^\dagger$ and $E_{\text{bottom}}^1 = \text{id}_{\text{MPO}}$. In practice, the computation of $\nabla \mathcal{L}$ consists of the following steps:

1. Perform a top-to-bottom sweep to compute and store all E_{top}^ℓ .
2. Perform a bottom-to-top sweep and consecutively compute all partial derivatives with respect to the gates in the layers $\ell = 1, \dots, L$.
 - (a) At each layer ℓ , first compute E_{bottom}^ℓ from the previous $E_{\text{bottom}}^{\ell-1}$. Only the current and previous bottom environments must be stored during this sweep.

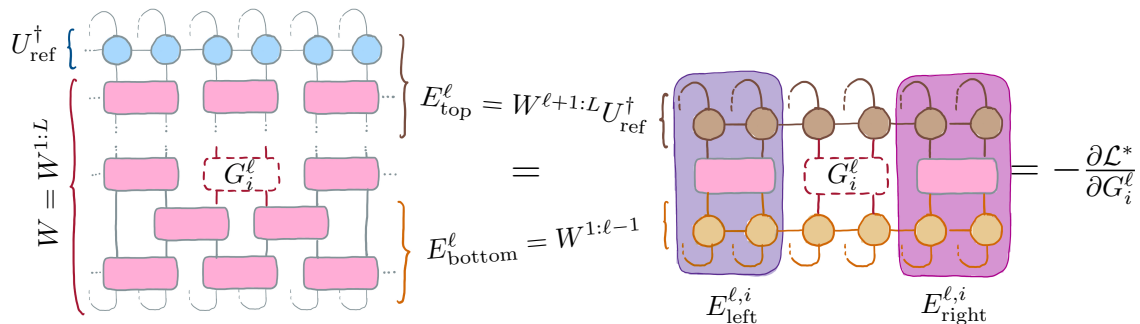


Figure 2: Diagrammatic sketch of the partial derivative $-\partial\mathcal{L}^*/\partial G_i^\ell$, where G_i^ℓ is the i -th gate in the ℓ -th layer of the brickwall circuit. The partial derivative can be obtained by “cutting out” the considered gate G_i^ℓ . For the efficient evaluation, a top environment MPO E_{top}^ℓ and a bottom environment MPO E_{bottom}^ℓ are computed. From there, the left and right environment, $E_{\text{left}}^{\ell,i}$ and $E_{\text{right}}^{\ell,i}$, are evaluated. Finally, contracting the resulting tensor network can compute the partial derivative.

- (b) Perform a right-to-left sweep to compute and cache $E_{\text{right}}^{\ell,i}$ for all $i = n_\ell, \dots, 1$.
- (c) Perform a left-to-right-sweep to compute each $\partial\mathcal{L}/\partial G_i^\ell$ by first computing $E_{\text{left}}^{\ell,i}$ from the previous $E_{\text{left}}^{\ell,i-1}$ and then contracting the resulting tensor network. Only the previous and current left environments have to be stored in this sweep.

The procedure of computing one partial derivative is visualized for a specific gate G_i^ℓ in Fig. 2. The Riemannian gradient $\nabla_{\text{Rie}}\mathcal{L}$ is then obtained through the projection given in Eq. (6) as discussed in Section III.

Computing the cost function in the context of tensor networks. The cost function is given by Eq. (1) with its variational part being representable by a tensor network contraction as given in Eq. (2). The latter can quickly be evaluated by contracting any partial derivative $\partial\mathcal{L}/\partial G_i^\ell$ with the corresponding “cut-out-gate” G_i^ℓ .

V. NUMERICAL SIMULATIONS

In the following, we consider (i) Hamiltonians of spin chains, and (ii) Hamiltonian of fermionic systems. We use the common notation of $(\sigma_i^1, \sigma_i^2, \sigma_i^3) = (X_i, Y_i, Z_i)$ for the vector of Pauli operators acting on the i -th qubit. Moreover, we denote in the context of second quantization the creation (annihilation) operator acting on orbital p as a_p^\dagger (a_p) and the corresponding number operator as $n_p = a_p^\dagger a_p$.

While our method can generally be applied to non-translationally invariant systems, we mainly consider systems with translational invariance for simplicity. However, we explicitly demonstrate this aspect for 10 disordered transverse-field Ising models on a one-dimensional chain with 20 sites. Furthermore, we show the optimization results for non-disordered transverse-field Ising and

Heisenberg models on a one-dimensional chain with 50 sites. Regarding the fermionic systems, we first show the optimization results for a non-disordered spinful Fermi-Hubbard model on a one-dimensional chain for 50 spin orbitals. As a proof of concept, we then demonstrate that our method can be applied to molecular Hamiltonians using the exemplary system of LiH. The utilized error measure \mathcal{C} is given by Eq. (1).

A. Spin systems

1. Transverse-field Ising model (non-disordered).

As a first example, we consider the transverse-field Ising model Hamiltonian on a chain with $N = 50$ sites and open boundary conditions:

$$H^{\text{Ising}} = \sum_{i=1}^{N-1} JZ_i Z_{i+1} + \sum_{i=1}^N (gX_i + hZ_i),$$

with $J, g, h \in \mathbb{R}$. In this study, we set without loss of generality $J = 1$ and $g = 0.75$, specifically considering the non-integrable case $h = 0.6$. We compute U_{ref} as 20 repetitions of a fourth-order Trotterization, $U_{\text{Trotter}}^{\text{IV},20}$, for a simulation time of $t = 2$, which is further compressed to a threshold of ϵ_{thres} . An overview of the reference error estimation is given in Table I.

The two-qubit Trotterization gates are given by

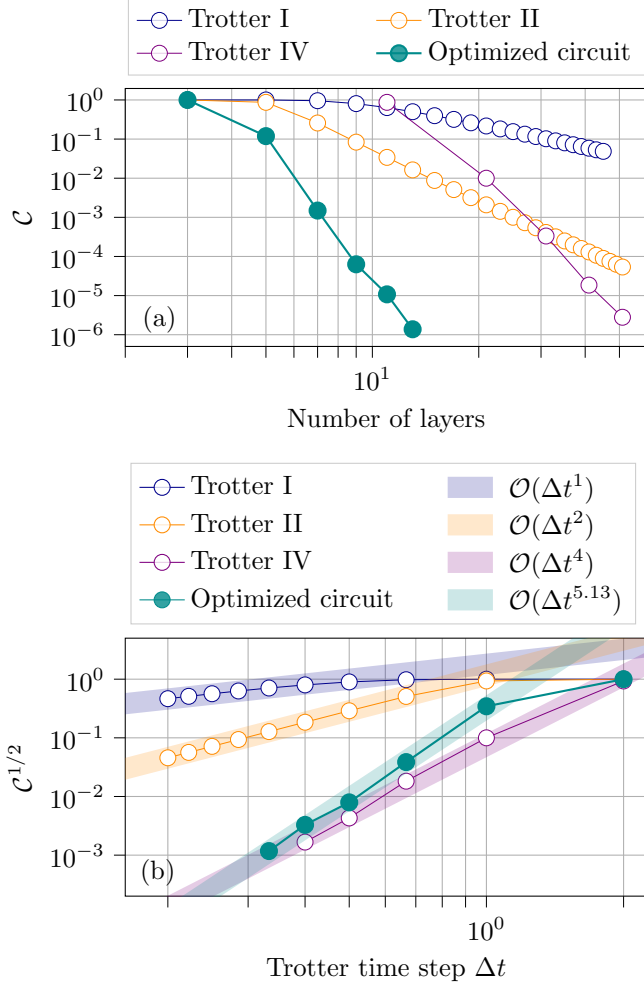
$$G^{\text{Ising}} = e^{-i\Delta t(JZZ + \frac{g_1}{2}XI + \frac{g_2}{2}IX + \frac{h_1}{2}ZI + \frac{h_2}{2}IZ)},$$

where

- $g = g_1 = g_2$ and $h = h_1 = h_2$ for gates in the middle of the circuit,
- $g_2 = g = \frac{g_1}{2}$ and $h_2 = h = \frac{h_1}{2}$ for gates that act on the first qubit, and

Table I: Overview of reference approximation for the different Hamiltonians.

	Reference approximation	Trotter error	Truncation error	Compression error
Transverse-field Ising	$U_{\text{Trotter}}^{\text{IV},20}$ ($t = 2$)	$4 \cdot 10^{-11}$	$2 \cdot 10^{-14}$	$2 \cdot 10^{-9}$
Heisenberg	$U_{\text{Trotter}}^{\text{IV},10}$ ($t = 0.25$)	$4 \cdot 10^{-11}$	$3 \cdot 10^{-14}$	$3 \cdot 10^{-11}$
Spinful Fermi-Hubbard	$U_{\text{Trotter}}^{\text{IV},10}$ ($t = 0.3$)	$2 \cdot 10^{-10}$	$5 \cdot 10^{-11}$	$3 \cdot 10^{-11}$

Figure 3: Results for the Ising model on a chain with $N = 50$ sites, $J = 1$, $g = 0.75$, $h = 0.6$, and $t = 2$.

(a) The error of the Riemannian optimized brickwall circuit compared to that of different Trotter circuits. (b) The error scaling in Trotter time step Δt for the Riemannian optimized brickwall circuit compared to that of various Trotter circuits.

- $g_1 = g = \frac{g_2}{2}$ and $h_1 = h = \frac{h_2}{2}$ for gates that act on the last qubit

due to the open boundary conditions.

The quantum circuits that are optimized are initialized as Trotterizations of order two. The optimization results and their comparison to Trotterizations of various orders

are shown in Fig. 3.

The Riemannian optimization method can increase the accuracy of each optimized quantum circuit with a relative error improvement, $\mathcal{C} = \mathcal{C}_{\text{init}}/\mathcal{C}_{\text{opt}}$, of up to four orders of magnitude as shown in Fig. 3(a). For example, the brickwall circuit with 12 layers could be optimized to an accuracy of five repetitions of a fourth-order Trotterization, which would initially require 51 layers. Furthermore, since all considered initial quantum circuits correspond to a Trotterization of order two, we can investigate the error scaling behavior with respect to the discretized Trotter time step Δt . For naive Trotterization of k -th order, the Trotter error scales like $\mathcal{O}(\Delta t^k)$. For the optimized brickwall circuit, we observe a scaling behavior of $\mathcal{O}(\Delta t^{5.13})$, i.e., a better scaling behavior for $\Delta t \ll 1$ than a fourth-order Trotterization. This analysis is shown in Fig. 3(b).

2. Transverse-field Ising model (disordered).

Unlike previous Riemannian quantum circuit optimization methods [13], our new method can also be applied to systems without translational invariance. To demonstrate this aspect, we consider a disordered modification of the prior Ising model:

$$H^{\text{Ising,dis}} = \sum_{i=1}^{N-1} J_i Z_i Z_{i+1} + \sum_{i=1}^N (g_i X_i + h_i Z_i)$$

with $J_i, g_i, h_i \in \mathbb{R}$, where we uniformly sample $J_i \in [\frac{J}{2}, \frac{3J}{2}]$, $g_i \in [\frac{g}{2}, \frac{3g}{2}]$, $h_i \in [\frac{h}{2}, \frac{3h}{2}]$ and without loss of generality J, g, h are chosen as in the translationally invariant case. We generate 10 different disordered Ising models of $N = 20$ sites and optimize each. The results for this setting are visualized in Fig. 4, where the optimization result for the corresponding non-disordered system is additionally displayed for comparison. Our method can handle disordered systems and achieves optimization results similar to those in the previous non-disordered case.

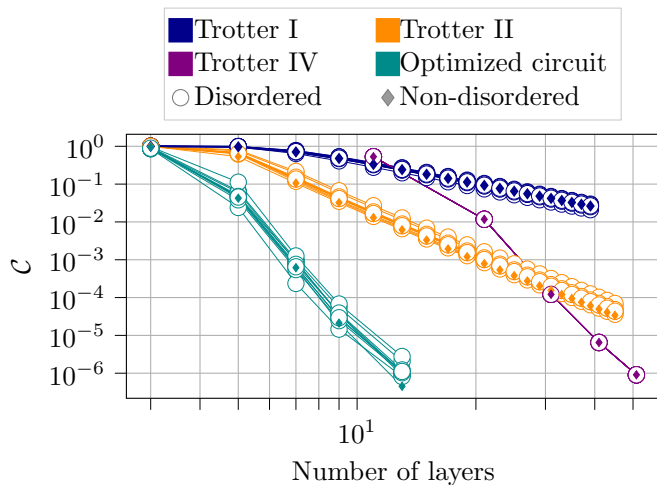


Figure 4: Results for the disordered Ising model on a one-dimensional chain of $N = 20$ sites. The corresponding non-disordered Ising model is plotted for reference for parameters $J = 1$, $g = 0.75$, $g = 0.6$, and $t = 2$. The parameters for the disordered models are uniformly sampled as $J_i \in [\frac{1}{2}J, \frac{3}{2}J]$, $g_i \in [\frac{1}{2}g, \frac{3}{2}g]$, and $h_i \in [\frac{1}{2}h, \frac{3}{2}h]$.

3. Heisenberg model.

As a second spin system, we consider the Heisenberg Hamiltonian on a chain of $N = 50$ sites:

$$H^{\text{Heis}} = \sum_{i=1}^{N-1} \sum_{\alpha=1}^3 J^\alpha \sigma_i^\alpha \sigma_{i+1}^\alpha + \sum_{i=1}^N \sum_{\alpha=1}^3 h^\alpha \sigma_i^\alpha,$$

with $\vec{J}, \vec{h} \in \mathbb{R}^3$. In the numerical simulations, we consider the parameters $\vec{J} = (1, 1, -\frac{1}{2})$ and $\vec{h} = (\frac{3}{4}, 0, 0)$. We compute U_{ref} as 10 repetitions of a fourth-order Trotterization, $U_{\text{Trotter}}^{\text{IV},10}$, for a simulation time of $t = 0.5$, which is further compressed to a threshold of ϵ_{thres} . An overview of the reference error estimation is given in Table I. The two-qubit Trotterization gates in the considered case are given by

$$G^{\text{Heis}} = e^{-i\Delta t (\frac{h_1}{2} XI + \frac{h_2}{2} IX + \sum_{\alpha=1}^3 J^\alpha \sigma_i^\alpha \sigma_{i+1}^\alpha)},$$

where

- $h_1 = \frac{3}{4} = h_2$ for quantum gates that do not act on any edge qubits,
- $h_2 = \frac{3}{4} = \frac{h_1}{2}$ for quantum gates that act on the first qubit, and
- $h_1 = h = \frac{h_2}{2}$ for quantum gates that act on the last qubit

due to the open boundary conditions.

We optimize various quantum circuits that are initialized as the most accurate Trotterization for the considered number of layers. In our case, these are Trotter

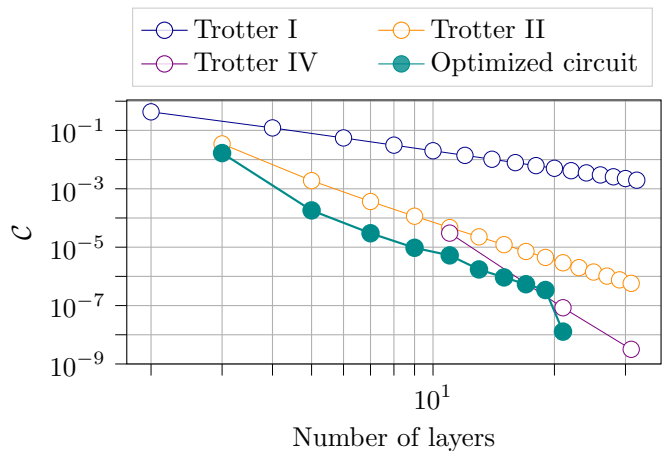


Figure 5: Results for the Heisenberg model on a chain with $N = 50$ sites, $\vec{J} = (1, 1, -\frac{1}{2})$, $\vec{h} = (\frac{3}{4}, 0, 0)$, and $t = 0.25$.

circuits of orders two and four. The numerical results are presented in Fig. 5. While the error improvement is not as significant as for the previous transverse-field Ising model, the Riemannian optimization increases the accuracy of all optimized quantum circuits to up to one order of magnitude.

B. Fermionic systems

When considering fermionic systems, their anti-symmetrical nature needs to be taken into account, e.g., utilizing second quantization. This study examines two types of fermionic Hamiltonians formulated in second quantization. A suitable fermion-to-qubit mapping such as the Jordan-Wigner transformation [31, 32] must be applied to map the corresponding operators. Furthermore, fermionic swaps must be considered when simulating longer-rang interactions using only nearest-neighbor two-qubit gates. Ref. [17] has introduced the fermionic swap network to simulate a Trotter step of a fermionic system using a brickwall circuit layout. In the following, we introduce the fermionic systems we considered for our numerical simulations and provide further details on the Trotter implementation in Appendix A.

1. Spinful Fermi-Hubbard model.

As a first fermionic system, we consider the one-dimensional spinful Fermi-Hubbard model given by

$$H^{\text{FH}} = - \sum_{\langle pq \rangle, s} T (a_{ps}^\dagger a_{qs} + a_{qs}^\dagger a_{ps}) + \frac{1}{2} \sum_p V n_{p\uparrow} n_{p\downarrow},$$

where $\langle pq \rangle$ denotes the pairs of adjacent spatial orbitals on a chain, and $s \in \{\uparrow, \downarrow\}$ denotes the spin. Within the

numerical simulations, we consider $T = 1$ and $V = 4$. We compute U_{ref} as 10 repetitions of a fourth-order Trotterization, $U_{\text{Trotter}}^{\text{IV},10}$, for a simulation time of $t = 0.3$, which is further compressed to a threshold of ϵ_{thres} as listed in Table I. To implement a Trotter step, a fermionic swap network is required, for which we provide more detail in Appendix A. We start from quantum circuits initialized in Trotter steps of the second or fourth order, where the best Trotterization is chosen for a given number of layers. The optimization results are visualized in Fig. 6.

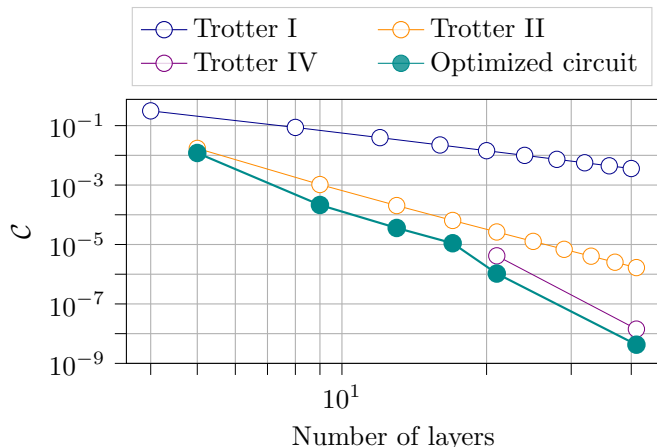


Figure 6: Results for the one-dimensional spinful Fermi-Hubbard model with $N = 50$ spin orbitals, $T = 1$, $V = 4$, and $t = 0.3$.

Again, the Riemannian optimization method can improve the simulation accuracy for each optimized quantum circuit. The presented results show a relative error improvement of up to a factor of 6.

2. Molecular Hamiltonian

The general molecular Hamiltonian in second quantization is given by

$$H^{\text{mol}} = \underbrace{\sum_{p,q=1}^N t_{pq} a_p^\dagger a_q}_T + \underbrace{\sum_{p,q,r,s=1}^N v_{pqrs} a_p^\dagger a_q^\dagger a_r a_s}_V,$$

where the scalar coefficients h_{pq} and h_{pqrs} are the one- and two-electron integrals. Various techniques can be employed to “diagonalize” the Coulomb interaction term V [33–36]. For the presented numerical experiment, we utilize the so-called *double factorization* [36], within which the two-body interaction term can be decomposed into diagonal terms via

$$V = \sum_{p,q} S_{pq} a_p^\dagger a_q + \sum_{\ell=1}^{N_{\text{rot}}} \sum_{i,j}^{\rho_\ell} \frac{\lambda_i^{(\ell)} \lambda_j^{(\ell)}}{2} n_i^{(\ell)} n_j^{(\ell)},$$

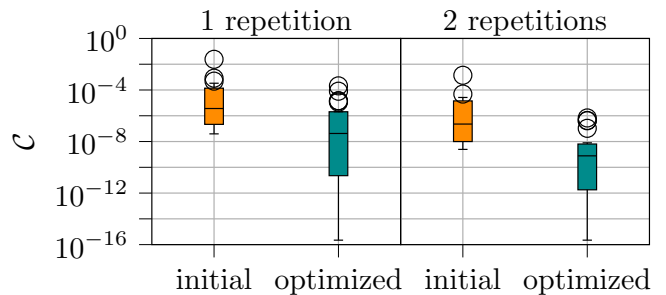


Figure 7: Riemannian optimization results for LiH. The optimization was performed on 21 diagonal molecular Hamiltonian terms. For each term, a brickwall circuit initialized as one repetition (left panel) or two repetitions (right panel) of a second-order Trotter step is optimized.

where

$$n_i^{(\ell)} = \sum_{p,s=1}^N U_{si}^{(\ell)} a_p^\dagger a_s U_{si}^{(\ell)} = a_{\psi_i^{(\ell)}}^\dagger a_{\psi_i^{(\ell)}}$$

corresponds to the number operator in a rotated basis, $\psi_i^{(\ell)} = \sum_{p=1}^N U_{pi}^{(\ell)} \phi_p$. By doing so, H^{mol} can be decomposed into G_{ivens} rotations and N_{rot} Hamiltonian terms

$$H_{\text{diag}}^{\text{mol},(\ell)} = \sum_{i,j} T_{ij}^{(\ell)} a_{\psi_i^{(\ell)}}^\dagger a_{\psi_j^{(\ell)}} + V_{ij}^{(\ell)} n_i^{(\ell)} n_j^{(\ell)},$$

where the two-body interaction $V^{(\ell)}$ is diagonal. A Trotter step for each $H_{\text{diag}}^{\text{mol},(\ell)}$ can be implemented following the fermionic swap network introduced in Ref. [17]. Again, we leave further details on the fermionic swap network in Appendix A. As a proof of concept, we consider the molecule LiH with six orbitals and a simulation time $t = 1$. We decompose its molecular Hamiltonian into $N_{\text{rot}} = 21$ sets of rotations and diagonal Hamiltonians $\{H_{\text{diag}}^{\text{mol},(\ell)}\}_{\ell=1}^{N_{\text{rot}}}$, of which we optimize each. We start from an initial quantum circuit corresponding to one and two Trotter steps of order 2. The optimization results are visualized in Fig. 7.

We observe that the simulation accuracy could be increased for each considered quantum circuit. In the best cases, the optimized errors become negligible on the order of numerical precision ($\approx 10^{-16}$). However, we do not claim any generalization of these results to larger systems, as the considered molecule is a simple example intended to serve as a proof of concept. In each optimization case, a relative error improvement of at least one order of magnitude could be achieved, with the best relative error improvement being eight orders of magnitude. The median relative error improvement is about two orders of magnitude.

VI. CONCLUSION

In this work, we present a novel approach that combines Riemannian optimization and tensor network methods to significantly enhance the simulation accuracy of initial Trotter circuits for the time evolution of various quantum systems. Our technique is purely classical, eliminating the need for costly quantum resources. To address the challenge of dimensionality in larger systems, we employ an MPO approximation for the reference time evolution operator. This requires careful selection of the maximum bond dimension and simulation time to ensure computational feasibility while maintaining accurate MPO representation of the actual time evolution. Our method is versatile and does not impose any symmetry constraints on the quantum systems. We demonstrate its effectiveness by optimizing ten disordered transverse-field Ising model instances. Additionally, we achieve error improvements of up to four orders of magnitude for one-dimensional systems such as the non-disordered transverse-field Ising model, the Heisenberg model, and the spinful Fermi-Hubbard model. We further showcase the applicability of our method to molecular Hamiltonians, using LiH as a proof of concept, where we achieve error improvements of up to eight orders of magnitude.

To tackle larger molecular systems, efficient methods to approximate the time evolution operator as an MPO are crucial [37, 38]. We leave a more detailed analysis of this aspect for future work. Our current method explicitly evaluates the cost function gradient through tensor network contractions and employs first-order Riemannian optimization. Future research could explore second-order optimization methods for brickwall circuits, such as

the trust-region algorithm [13, 39], potentially using automatic differentiation to evaluate the gradient and Hessian [18].

ACKNOWLEDGMENTS

We thank Joe Gibbs for valuable discussions about his recent work in Ref. [15]. We further thank Yu Wang for his input on tensor network methods. The Riemannian ADAM optimizer was implemented based on the ADAM implementation of `qiskit v0.18` [40]. All tensor network operations were implemented using `jax.numpy` [41]. S.S. acknowledges support from the BMW group. The authors gratefully acknowledge the computational and data resources provided by the Leibniz Supercomputing Centre (www.lrz.de).

Data availability

The implementation used in this project, as well as the numerical results and a script to generate the figures in this publication, are available under <https://github.com/INMLe/rqcopt-mpo>.

Authors contribution

I.L. implemented the tensor network and optimization framework and performed the numerical simulations. S.S. implemented the double factorization of the molecular Hamiltonian. I.L. wrote the manuscript with contributions from all authors. C.M. supervised the project.

-
- [1] R. P. Feynman, Simulating physics with computers, in *Feynman and computation* (cRc Press, 2018) pp. 133–153.
 - [2] S. Lloyd, Universal quantum simulators, *Science* **273**, 1073 (1996).
 - [3] C. Zalka, Simulating quantum systems on a quantum computer, *Proceedings of the Royal Society of London. Series A: Mathematical, Physical and Engineering Sciences* **454**, 313 (1998).
 - [4] B. Bauer, S. Bravyi, M. Motta, and G. K.-L. Chan, Quantum algorithms for quantum chemistry and quantum materials science, *Chemical Reviews* **120**, 12685 (2020).
 - [5] Y. Cao, J. Romero, J. P. Olson, M. Degroote, P. D. Johnson, M. Kieferová, I. D. Kivlichan, T. Menke, B. Peropadre, N. P. Sawaya, *et al.*, Quantum chemistry in the age of quantum computing, *Chemical reviews* **119**, 10856 (2019).
 - [6] J. Eisert, M. Friesdorf, and C. Gogolin, Quantum many-body systems out of equilibrium, *Nature Physics* **11**, 124 (2015).
 - [7] G. Kluber, Trotterization in quantum theory, *arXiv preprint arXiv:2310.13296* (2023).
 - [8] A. M. Childs, Y. Su, M. C. Tran, N. Wiebe, and S. Zhu, Theory of trotter error with commutator scaling, *Physical Review X* **11**, 011020 (2021).
 - [9] R. Mansuroglu, T. Eckstein, L. Nützel, S. A. Wilkinson, and M. J. Hartmann, Variational hamiltonian simulation for translational invariant systems via classical preprocessing, *Quantum Science and Technology* **8**, 025006 (2023).
 - [10] R. Mansuroglu, F. Fischer, and M. J. Hartmann, Problem-specific classical optimization of hamiltonian simulation, *Physical Review Research* **5**, 043035 (2023).
 - [11] M. S. Tepaske, D. Hahn, and D. J. Luitz, Optimal compression of quantum many-body time evolution operators into brickwall circuits, *SciPost Physics* **14**, 073 (2023).
 - [12] C. Mc Keever and M. Lubasch, Classically optimized hamiltonian simulation, *Physical review research* **5**, 023146 (2023).
 - [13] A. Kotil, R. Banerjee, Q. Huang, and C. B. Mendl, Riemannian quantum circuit optimization for hamiltonian simulation, *Journal of Physics A: Mathematical and Theoretical* **57**, 135303 (2024).
 - [14] L. Causer, F. Jung, A. Mitra, F. Pollmann, and A. Gammon-Smith, Scalable simulation of nonequilib-

- rium quantum dynamics via classically optimized unitary circuits, *Physical Review Research* **6**, 033062 (2024).
- [15] J. Gibbs and L. Cincio, Deep circuit compression for quantum dynamics via tensor networks, *arXiv preprint arXiv:2409.16361* (2024).
- [16] P. K. Diederik, Adam: A method for stochastic optimization, (*No Title*) (2014).
- [17] I. D. Kivlichan, J. McClean, N. Wiebe, C. Gidney, A. Aspuru-Guzik, G. K.-L. Chan, and R. Babbush, Quantum simulation of electronic structure with linear depth and connectivity, *Physical review letters* **120**, 110501 (2018).
- [18] D. Rogerson and A. Roy, Quantum circuit optimization using differentiable programming of tensor network states, *arXiv preprint arXiv:2408.12583* (2024).
- [19] I. Luchnikov, A. Ryzhov, S. Filippov, and H. Ouerdane, Qgopt: Riemannian optimization for quantum technologies, *Scipost physics* **10**, 079 (2021).
- [20] I. A. Luchnikov, M. E. Krechetov, and S. N. Filippov, Riemannian geometry and automatic differentiation for optimization problems of quantum physics and quantum technologies, *New Journal of Physics* **23**, 073006 (2021).
- [21] E. Godinez-Ramirez, R. Milbradt, and C. B. Mendl, A riemannian approach to the lindbladian dynamics of a locally purified tensor network, *arXiv preprint arXiv:2409.08127* (2024).
- [22] R. Wiersema and N. Killoran, Optimizing quantum circuits with riemannian gradient flow, *Physical Review A* **107**, 062421 (2023).
- [23] M. Casanova, K. Ohki, and F. Ticozzi, Finding quantum codes via riemannian optimization, *arXiv preprint arXiv:2407.08423* (2024).
- [24] Y. Yao, F. Miatto, and N. Quesada, Riemannian optimization of photonic quantum circuits in phase and fock space, *SciPost Physics* **17**, 082 (2024).
- [25] S. Ahmed, F. Quijandria, and A. F. Kockum, Gradient-descent quantum process tomography by learning kraus operators, *Physical Review Letters* **130**, 150402 (2023).
- [26] M. Hauru, M. Van Damme, and J. Haegeman, Riemannian optimization of isometric tensor networks, *Scipost physics* **10**, 040 (2021).
- [27] P.-A. Absil, R. Mahony, and R. Sepulchre, *Optimization algorithms on matrix manifolds* (Princeton University Press, 2008).
- [28] A. Edelman, T. A. Arias, and S. T. Smith, The geometry of algorithms with orthogonality constraints, *SIAM journal on Matrix Analysis and Applications* **20**, 303 (1998).
- [29] G. Bécigneul and O.-E. Ganea, Riemannian adaptive optimization methods, *arXiv preprint arXiv:1810.00760* (2018).
- [30] U. Schollwöck, The density-matrix renormalization group in the age of matrix product states, *Annals of physics* **326**, 96 (2011).
- [31] I. Duck, W. Pauli, and E. Sudarshan, *Pauli and the spin-statistics theorem* (World Scientific, 1997).
- [32] P. Jordan and E. P. Wigner, About the Pauli exclusion principle, *Z. Phys.* **47**, 631 (1928).
- [33] R. Babbush, N. Wiebe, J. McClean, J. McClain, H. Neven, and G. K.-L. Chan, Low-depth quantum simulation of materials, *Physical Review X* **8**, 011044 (2018).
- [34] S. R. White, Hybrid grid/basis set discretizations of the schrödinger equation, *The Journal of chemical physics* **147** (2017).
- [35] M. Luo and J. I. Cirac, Efficient simulation of quantum chemistry problems in an enlarged basis set, *arXiv preprint arXiv:2407.04432* (2024).
- [36] M. Motta, E. Ye, J. R. McClean, Z. Li, A. J. Minnich, R. Babbush, and G. K.-L. Chan, Low rank representations for quantum simulation of electronic structure, *npj Quantum Information* **7**, 83 (2021).
- [37] S. Paeckel, T. Köhler, A. Swoboda, S. R. Manmana, U. Schollwöck, and C. Hubig, Time-evolution methods for matrix-product states, *Annals of Physics* **411**, 167998 (2019).
- [38] M. Van Damme, J. Haegeman, I. McCulloch, and L. Vanderstraeten, Efficient higher-order matrix product operators for time evolution, *SciPost Physics* **17**, 135 (2024).
- [39] F. Putterer, M. M. Zumpé, I. N. M. Le, Q. Huang, and C. B. Mendl, High performance contraction of quantum circuits for riemannian optimization, In preparation (2025).
- [40] *ADAM implementation by qiskit v0.18* (2021).
- [41] J. Bradbury, R. Frostig, P. Hawkins, M. J. Johnson, C. Leary, D. Maclaurin, G. Necula, A. Paszke, J. VanderPlas, S. Wanderman-Milne, and Q. Zhang, *JAX: composable transformations of Python+NumPy programs* (2018).

Appendix A: Fermionic swap network

In this work, Trotter circuits of first-, second-, and fourth-order are considered. Given a Hamiltonian of the form $H = \sum_{i=1}^k H_i$, these Trotterizations are given by [7]

$$\begin{aligned}
 U_1(t) &= \prod_{i=1}^k e^{-iH_i t}, \\
 U_2(t) &= \prod_{i=1}^k e^{-iH_i t/2} \prod_{i=k}^1 e^{-iH_i t/2}, \\
 U_4(t) &= [U_2(s_2 t)]^2 [U_2((1 - 4s_2)t)] [U_2(s_2 t)]^2,
 \end{aligned}$$

where in the latter $s_2 = (4 - 4^{1/3})^{-1}$.

To implement a Trotter circuit for fermionic Hamiltonians, each orbital p is represented by a qubit i_p and the fermionic operators a^\dagger, a, n need to be mapped to corresponding qubit operators [17]. Using the Jordan-Wigner transformation [31, 32] for this purpose results in possibly long-range Pauli- Z strings. However, if the qubits representing the involved orbitals p, q are adjacent, i.e., $i_q = i_p + 1$, the time-evolution of a single summand in V can be implemented by two-qubit gates. To this end, a fermionic swap network architecture can be employed [17], where fermionic swaps

$$f_{\text{swap}} = \begin{pmatrix} 1 & 0 & 0 & 0 \\ 0 & 0 & 1 & 0 \\ 0 & 1 & 0 & 0 \\ 0 & 0 & 0 & -1 \end{pmatrix}$$

are utilized suitably.

1. Spinful Fermi-Hubbard model

For simplicity, we state the considered one-dimensional spinful Fermi-Hubbard Hamiltonian again:

$$H^{\text{FH}} = - \sum_{\langle pq \rangle, s} T_{pq} (a_{ps}^\dagger a_{qs} + a_{qs}^\dagger a_{ps}) + \frac{1}{2} \sum_p V_p n_{p\uparrow} n_{p\downarrow}.$$

As can be seen, interactions of spin orbitals (ps) and (qs) for $p = q + 1$ as well as interactions between spin orbitals ($p \uparrow$) and ($p \downarrow$) need to be considered. To simulate a Trotter step, we order the spin orbitals as follows (example of 5 spatial orbitals):



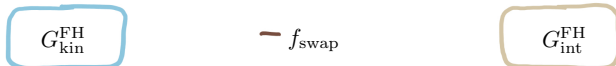
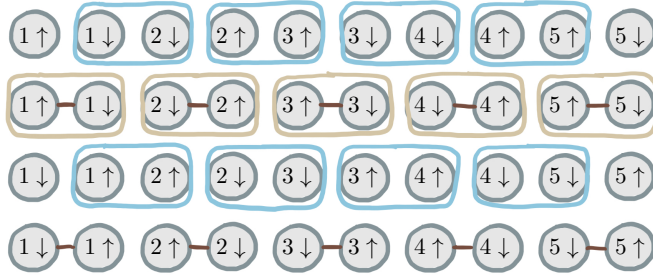
We then construct the swap network as follows: The first and third layer simulate the kinetic hopping terms, for which the two-qubit gates V_{kin} after Jordan-Wigner transformation are given by

$$G_{\text{kin}}^{\text{FH}}(i_p, i_q) = \begin{pmatrix} 1 & 0 & 0 & 0 \\ 0 & \cos(T_{pq}\Delta t) & i \sin(T_{pq}\Delta t) & 0 \\ 0 & i \sin(T_{pq}\Delta t) & \cos(T_{pq}\Delta t) & 0 \\ 0 & 0 & 0 & 1 \end{pmatrix}.$$

The second layer simulates the on-site interactions while simultaneously swapping the corresponding orbitals, for which the two-qubit gates V_{int} after applying Jordan-Wigner transformation are given by

$$G_{\text{int}}^{\text{FH}}(i_p, i_q) = \begin{pmatrix} 1 & 0 & 0 & 0 \\ 0 & 0 & 1 & 0 \\ 0 & 1 & 0 & 0 \\ 0 & 0 & 0 & -e^{-iV_{pq}\Delta t} \end{pmatrix}.$$

Note that for first-order Trotterization, an additional layer that reverses the previous fermionic swaps given by needs to be applied, which is not necessary for even-order Trotterizations. The fermionic swap network for a first-order Trotter step of a system with 10 spin orbitals is then given by:



2. Molecular Hamiltonian

Ref. [17] presented a fermionic swap network to implement a Trotter step of a molecular Hamiltonian with diagonal interaction term given by

$$H = \sum_{pq} T_{pq} a_p^\dagger a_q + \frac{1}{2} \sum_{p \neq q} V_{pq} n_p n_q,$$

where p, q denote the orbitals. In this case, the interaction and kinetics between two neighboring orbitals as well as their fermionic swapping can be jointly simulated by the following two-qubit gate:

$$f_{\text{sim}}(i_p, i_q) = \begin{pmatrix} 1 & 0 & 0 & 0 \\ 0 & -i \sin(T_{pq}\Delta t) & \cos(T_{pq}\Delta t) & 0 \\ 0 & \cos(T_{pq}\Delta t) & -i \sin(T_{pq}\Delta t) & 0 \\ 0 & 0 & 0 & -e^{-iV_{pq}\Delta t} \end{pmatrix}.$$

The following fermionic swap network implements a Trotter step of first-order for 6 orbitals, where the layers for reversing the orbital ordering are neglected for simplicity:

